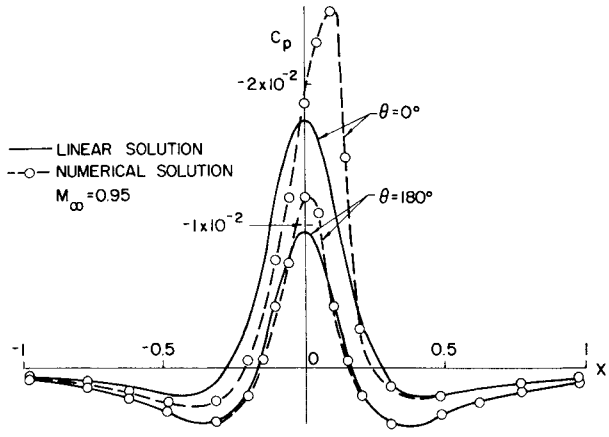

Fig. 4 Pressure distribution along typical meridian planes for supercritical conditions.

Technology Labs., Inc., and based on a modification of the method of Murman and Cole.[2] The modification, discussed in Ref. 3, consists in transforming the infinite domain around a two-dimensional shape into a finite one by the transformations $\xi = \tanh \alpha x$ and $\eta = 1 - e^{-\beta r}$, so that exact boundary conditions can be applied at the boundaries $\xi = \pm 1$ and $\eta = +1$, that is at the infinity of the physical plane. In the present case, the finite domain around a quasi-cylindrical surface is defined by $-1 \leqq \xi \leqq 1$ and $\eta_1 \leqq \eta \leqq 1$ where η_1 is the value of η for $r = R$.

Examples

To test the method, we have first compared a numerical solution with an exact analytical solution. We have computed analytically, using linear theory, the pressure coefficient and the velocity v induced along the cylindrical surface $r = R$ by the doublet-horseshoe vortex configuration shown in Fig. 1. Using as boundary condition along the surface $r = R$ the computed v (which, at any x can be shown to be adequately represented by four harmonics in θ) and using the potential induced by the horseshoe vortex as boundary condition at infinity around the cylinder, we have then solved numerically the linearized version of Eq. (4) along the four planes $\theta = 0°$, 60°, 120°, and 180°. Typical comparisons of C_p at $r = R$ are shown in Figs. 2 and 3. The numerical solution has converged after 200 iterations with a grid network of 41×20 points in each plane.

As a second step, a nonlinear, supercritical case has been analyzed numerically, by using as boundary condition at $r = R$ the Φ_y provided from linear theory by the same wing-body configuration of Fig. 1 with $M_\infty = 0.95$ and $C_L = 0.7$. At infinity around the cylinder, the boundary conditions that have been used are $\Phi_x = 0$ along the plane $x = \infty$ and $\Phi = 0$ everywhere else. By solving again Eq. (4) in the planes $\theta = 0°$, 60°, 120°, and 180°, the resulting pressure distributions at $r = R$ and along typical meridian planes are shown in Fig. 4 and compared with the analytical linear solutions. The supersonic pockets in the several meridian planes are shown in Fig. 5. Because of the courseness

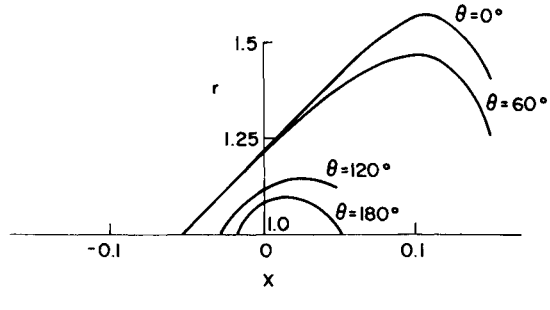

Fig. 5 Contour of supersonic region in several meridian planes.

of the grid network that has been used (41×20 points) the supersonic region is identified by only a few grid points and the shock has been smeared through a relatively large region of the flow. A finer resolution could have been obtained with a finer mesh.

It appears from these few examples that the method can be used advantageously to determine the flowfield around quasi-cylindrical shapes (lifting and nonlifting). Its application to other configurations, such as channel flows and flow around finite bodies without axial symmetry can also proceed in a similar manner. Similarly, the method can be extended to the complete nonlinear transonic equation with nonlinear boundary conditions.

References

[1] Ferri, A., "The Linearized Characteristic Method and Its Application to Practical Nonlinear Supersonic Problems," Rept. 1102, 1951, NACA.

[2] Murman, E. N. and Cole, J. D., "Calculation of Plane Steady Transonic Flows," *AIAA Journal*, Vol. 9, No. 1, Jan. 1971, pp. 114–121.

[3] Baronti, P., Elzweig, S., and Vaglio-Laurin, R., "Transonic Flows by Coordinate Transformation," *AIAA Journal*, Vol. 9, No. 11, Nov. 1971, p. 2280.

Photographic Observations of CW HF Chemical Laser Reacting Flowfield

R. L. VARWIG*
The Aerospace Corporation, El Segundo, Calif.

Introduction

THE luminosity of the gas from the reaction $F + H_2 \rightarrow HF(v) + H$ in the reacting region of an HF chemical laser permits photographic observation of fluid dynamic flow phenomena. More extensive observations are presented in Ref. 1.

The triple-slit nozzle configuration described in Ref. 2 was used in this study (Fig. 1). The primary nozzle from which He and F atoms emerge is a wedge-shaped nozzle nominally 0.020×0.500 in. at throat cross section, 0.625 in. long, and 0.254×0.500 in. at exit cross section. H_2 fuel is injected from

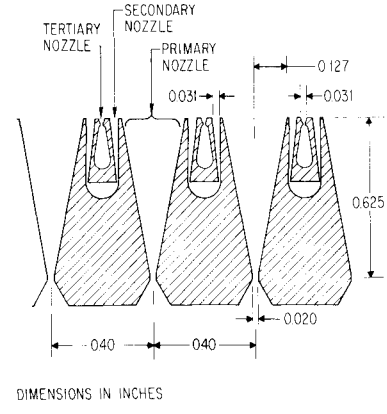

Fig. 1 Portion of the 16-nozzle triple-slit nozzle bank showing gas injection scheme.

Received May 6, 1974; revision received May 30, 1974. This work was supported by the U.S. Air Force under Contract F04701-73-C-0074. The author gratefully acknowledges helpful discussions with H. Mirels and W. R. Warren Jr.

Index categories: Reactive Flows; Lasers.

* Staff Scientist. Member AIAA.

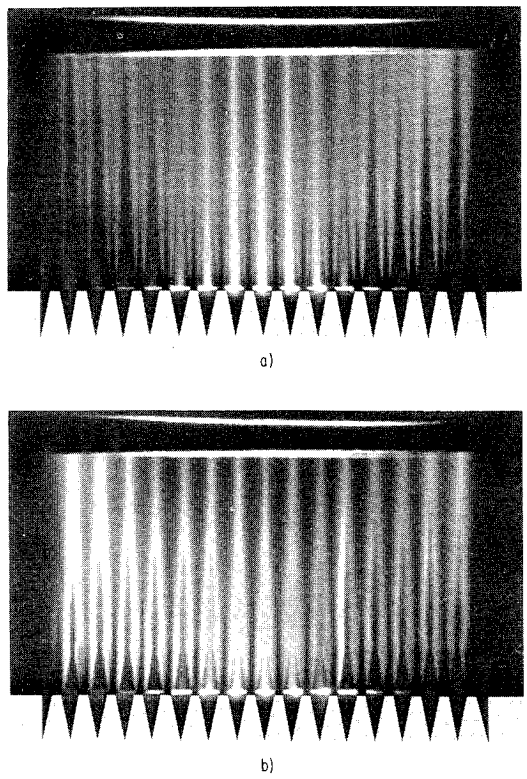

Fig. 2 Effect of downstream cavity pressure on nozzle flowfield: a) cavity pressure = 3.5 torr, the nozzle exit static pressure; b) cavity pressure = 7 torr, twice nozzle exit static pressure.

tertiary slit nozzles located between the primary nozzles. A buffer gas that consists of He plus varying amounts of H_2 is injected from secondary nozzles so that the H_2 fuel can be isolated from the oxidizer in the primary nozzle.

The primary flow consisted of 4.3 g/sec of SF_6 in a carrier gas of 2.0 g/sec of He with 0.8 g/sec of O_2. Nozzle plenum pressure was 1.2 atm for most of the tests, while total temperature obtained by electric arc heating was ~1850 K. For these plenum conditions, the nozzle exit (centerline) Mach number M was 5, and the exit static pressure was 4 torr. H_2 flow from the tertiary nozzle varied from 0.1 to 1.6 g/sec, providing a range of tertiary nozzle exit static pressure from less than half to more than twice the 4 torr of the primary nozzle flow. Secondary nozzle flow was either zero or 1 g/sec each of He and H_2. Cavity ambient pressure was varied from about a half, equal to, and twice the primary nozzle exit free-stream pressure. In wind-tunnel terms, the primary nozzle flow was therefore underexpanded, matched, and overexpanded.

Experimental Results and Discussion

Typical of the photographic observations are the flow pictures of Fig. 2. For such flowfields, the plenum conditions and component mass flows were held constant, and the downstream cavity pressure was varied from 1.6 to 3.5 to 7 torr, respectively, i.e., half, equal to, and twice the primary nozzle exit static pressure. There was no secondary flow. In these photographs, the luminous layer observed is assumed to be the reacting region. The leading edge is expected to mark the extent of the mixing of the fuel and oxidant streams.

As the reactant gases mix at their boundary, the consequent exothermic reaction increases the temperature and decreases the density in the reaction zone. The lateral expansion of the heated gases creates a "displacement thickness" effect,[3,4] and shock waves are generated from the corresponding deflection of the supersonic nozzle flow. In these tests, the primary nozzles are wedge shaped, and the flow downstream of the nozzles is diverging. Therefore, even for nonreacting flow, a pair of shock waves must form downstream of each nozzle in order to satisfy boundary conditions with the adjacent H_2 stream or symmetry boundary conditions between adjacent primary nozzles. Both of these effects must be present in these tests. In addition, since the flows are not parallel streams, the shock waves produced must be curved. One can estimate the location of a shock wave by noting its intersection with the luminous front of the reacting layer. The intersection appears as a discontinuity in the slope of the luminous edge. It should be noted that the intersection of the shock wave with the luminous front of the reacting layer moves upstream as the cavity ambient pressure increases relative to the nozzle exit static pressure as shown in Fig. 2.

From such observations as these, the shock angle measured relative to the flow direction, which is assumed on the average to be half the nozzle wall angle, for the flow of Fig. 2a is 17°. Hence, the flow deflection angle behind the shock should be ~7°. For the flow conditions in Fig. 2b where the downstream cavity pressure is twice the nozzle exit static pressure, the shock wave angle is 22°. Associated with this shock wave angle is a flow deflection behind the shock of 12°, or 5° more than that for the case where the ambient cavity pressure is equal to the primary nozzle exit static pressure. That is, the flow for the conditions in Fig. 2a is little more than straightened near the nozzle edges, while for the conditions in Fig. 2b the flow is actually deflected toward the center of the primary nozzle.

Despite the presence of oblique shocks, it is of interest to compare the lateral propagation of the luminous front with laminar and turbulent diffusion estimates. For laminar diffusion, the edge of the reaction zone should have the shape

$$\delta_L = A(Dx/u)^{1/2} \tag{1}$$

where δ_L is the ordinate, x is the streamwise distance, u is the streamwise velocity, D is the diffusion coefficient, and A is a dimensionless quantity of order 1, which depends on the stoichiometry and geometry of the mixing streams. For laminar diffusion of H_2 into He

$$D = 2.88 \times (10^{-4}T^{3/2}/p) \quad (\text{cm}^2/\text{sec}) \tag{2}$$

where T is in degrees Kelvin and p is in atmospheres.[5]

For turbulent diffusion

$$\delta_T = \bar{A}x \tag{3}$$

where $\bar{A}$ is of order 0.1.

The experimental variation of δ with x was obtained through measurement of the distance d between the luminous fronts advancing from each side of the primary nozzle as a function of distance from the nozzle exit. The distance d was subtracted

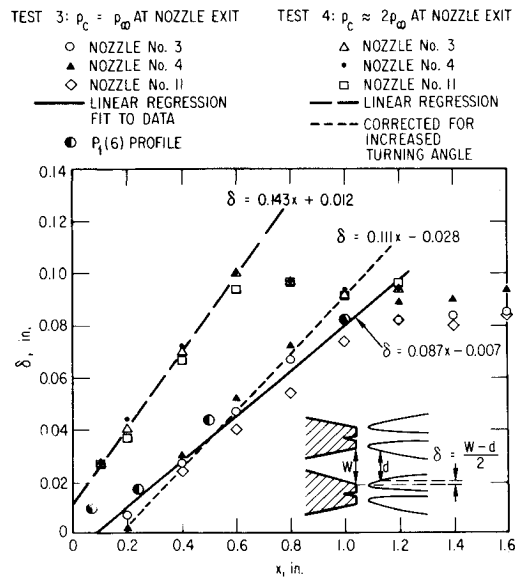

Fig. 3 Position of luminous front in primary nozzle flow for cavity pressure equal to and greater than nozzle exit static pressure.

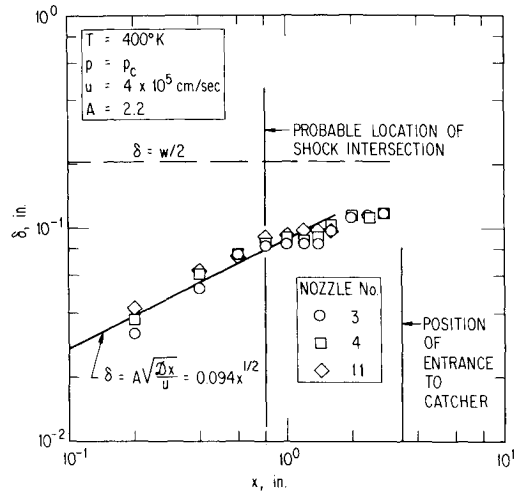

Fig. 4 Position of luminous front in primary nozzle flow for cavity pressure equal to nozzle exit static pressure with secondary flow of 1 g/sec each He and H_2 injected.

from the nozzle width w, and the difference was divided by two as indicated in Fig. 3.

For tests in which there was no flow in the secondary nozzles, the rate of growth of the reaction zone appeared to be linear. When the exit pressures in the primary and tertiary nozzles were equal [Fig. 2a] the constant of proportionality $\bar{A}$ was approximately 0.09 (Fig. 3, solid curve), which is remarkably close to the nominal value for turbulent mixing.[6] When the ambient cavity pressure was larger than the nozzle exit freestream pressure [Fig. 2b], the growth of the reaction zone was steeper as shown in Fig. 3 by the dashed line curve, which represents a linear least squares fit to the data. The shock waves can be estimated from Figs 2a and 2b as previously noted, and the difference in flow deflection angle obtained. By subtracting the difference in turning angle from the regression line of the data for Fig. 2b and translating the line to account for the shock wave originating further upstream, we obtained a curve that fell within the scatter of the data from Fig. 2a ($p = p_c$). Although the line does not have the same slope as the linear regression line fitted to these data, it is closer to that slope (0.11 corrected from 0.14 compared to 0.09) than the value uncorrected for turning angle difference. Apparently, the larger angle of growth of the reaction zone associated with flows with high ambient pressure relative to nozzle exit static pressure is closely related to the strength of the shock wave associated with the flow.

When a secondary flow consisting of half He and half H_2 was introduced and the exit pressures were matched, the growth of luminous front appeared to be proportional to $x^{1/2}$ (Fig. 4), i.e., laminar according to Eq. (1). Computation of A from these measurements yields either 4.7 or 2.2, depending on whether D/u is evaluated on the basis of conditions at the nozzle exit or those more characteristic of the cavity further downstream. Conditions further downstream were taken from Ref. 7. These are $T = 400$ K, $p = p_c$, the downstream cavity pressure, and $u = 3 \times 10^5$ cm/sec.

Thus, both laminar and turbulent mixing characteristics have been observed. The presence of laminar mixing appears to require matched exit pressures and the absence of a significant base region, i.e., when there was no flow in the secondary nozzles, these nozzles correspond to a base region between the primary and tertiary nozzles.

Whether emission from the visible overtones in these observations actually represents the leading edge of the mixing and reacting gas layers is not clearly evident. To examine this question a spectrographic measurement was made. The $P_1{}^6$ line of the P rotational branch of the 1 to 0 vibrational transition of the HF molecule at 2.708 μ was observed for flow conditions similar to those of Test 3 of Fig. 3. From these observations a spreading rate of the mixing and reacting flow can be obtained from which an equivalent to the luminous front position of the photographic observations can be determined. When such data were plotted on Fig. 3 they appeared to fall within the scatter of the data obtained from the photographic observations for Test 3 conditions. Consequently, one would conclude that the photographic method can provide measurements that well represent the location of the mixing and reacting front.

Since this study was completed, the work of Shackleford et al.[8] has been reported. These mixing studies used two large-scale nozzles. Mixing was between parallel flows of reactant gases, and the diluent gas was N_2 rather than He. Also, nozzle geometry differed significantly, e.g., Shackleford has no base region between nozzles, making comparison between the two studies difficult. Both Shackleford's studies and this one isolated conditions of laminar and turbulent mixing: the studies of Ref. 8 examined the effect of the Reynolds number, while the present study effectively varied mixing geometry. Nevertheless, for laminar mixing both works showed reaction layer growth proportional to $x^{1/2}$, and for turbulent flows agreement for the value $\bar{A}$ is good (0.09 compared with 0.08).

References

[1] Varwig, R. L., "Photographic Observations of CW HF Chemical Laser Reacting Flow Field," TR-0073(3250-10)-8, Nov. 1972, The Aerospace Corp., El Segundo, Calif.

[2] Durran, D. A. and Varwig, R. L., "Performance of Triple Slit Nozzle for Chemical Laser Applications," TR-0073(3240-10)-3, Oct. 1972, The Aerospace Corp., El Segundo, Calif.

[3] Warren, W. R., Jr., "Reacting Flow and Pressure Recovery Processes in HF/DF Chemical Lasers," presented at 4th International Colloquium on Gas Dynamics of Explosions and Reactive Systems, Univ. of California at San Diego, July 10–13, 1973.

[4] Ellinwood, J. W. and Mirels, H., "Laminar Flamesheet With Hypersonic Viscous Interaction," *AIAA Journal*, Vol. 10, No. 6, June 1972, pp. 830–832.

[5] Mirels, H., Hofland, R., and King, W. S., "Simplified Model of CW Diffusion-Type Chemical Laser," *AIAA Journal*, Vol. 11, No. 2, Feb. 1973, pp. 156–164.

[6] Schlichting, H., *Boundary Layer Theory*, 4th ed., McGraw-Hill, New York, 1960, pp. 598–600.

[7] Varwig, R. L. and Kwok, M. A., "CW HF Chemical Laser Flow Diagnostic Measurements," *AIAA Journal*, Vol. 12, No. 2, Feb. 1974, pp. 208–212.

[8] Shackleford, W. L., Witte, A. B., Broadwell, J. E., Trost, J. E., Jacobs, T. A., "Experimental Studies of Chemically Reactive ($F+H_2$) Flow in Supersonic Free Jet Mixing Layers," *AIAA Journal*, Vol. 12, No. 8, Aug. 1974, pp. 1009–1010.

Improved Approximation of Constitutive Elasto-Plastic Stress-Strain Relationship for Finite Element Analysis

T. R. Hsu* and A. W. M. Bertels†
University of Manitoba, Winnipeg, Canada

With the increasing demand of nuclear power and aerospace applications, the elasto-plastic stress analysis of solid structures has become absolutely necessary. Finite element analysis has shown to be one of the most promising and practical methods for these applications as illustrated in Ref. 1.

Since the relationship of stress vs strain is nonlinear for material undergoing plastic deformation, constant change of the

Received May 3, 1974.
Index categories: Aircraft Structural Design (Including Loads); Structural Static Analysis.

* Associate Professor, Department of Mechanical Engineering.
† Senior Research Associate, Department of Mechanical Engineering.